

Pt, Co, Fe and Ni Nan particles on Micro/Nano-Structured Carbon for the Methanol Electro-Oxidation in Acid Medium

D. Macias Ferrer^{1*}, J.A. Melo Banda¹, R. Silva Rodrigo¹, M. Lam Maldonado¹, M.A. Meraz-Melo², J.Y. Verde Gómez³, U. Páramo García¹, N.P. Díaz Zavala¹

¹Centro de Investigación en Petroquímica, TecNM/Instituto Tecnológico de Cd. Madero, Cd. Madero Tamaulipas, México

²Departamento de Ingeniería, TecNM/Instituto Tecnológico de Iztapalapa III, Ciudad de México, México

³División de Estudios de Posgrado, Tecnológico Nacional de México/ Instituto Tecnológico de Cancún, Cancún Quintana Roo, 77515, México

Corresponding Author: D. Macias Ferrer

ABSTRACT : In this work, Pt, Co, Fe and Ni nanoparticles supported on micro/nano-structured carbon (MNC) were tested in methanol electro-oxidation process in acid medium. The samples Pt/MNC, Co/MNC, Fe/MNC and Ni/MNC (10 wt % metal loading), were synthesized by impregnation method and chemical reduction route using citric acid as dispersing agent, ammonium hydroxide and a static atmosphere of Ar-H₂ as reductant agents. MNC sample was synthesized via nanocasting process with anhydrous pyrolysis at 900 °C using SBA-15 as hard template and refined sugar as carbon source. SBA-15 was prepared via sol gel using pluronic P-123 as surfactant and tetraethoxysilane as silica precursor. The samples were characterized by means of BET, FTIR, Raman, XRD, XPS, SEM and EDS. The electrochemical measurements were carrying out by cyclic voltammetry (CV) in 0.5M H₂SO₄ + 1.0M CH₃OH at 20 mV/s and 10 cycles.

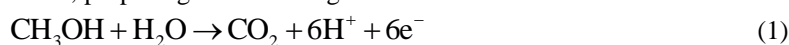
KEYWORDS – SBA-15, methanol electro-oxidation, Micro/nano structured carbon, nanoparticles, nanocasting

Date of Submission: 14-06-2018

Date of acceptance: 29-06-2018

I. INTRODUCTION

Due to the high energy density of methanol, methanol oxidation reaction (MOR) has been exhaustively studied since 1930, starting with the works of Schreiner [1]. This electrochemical process of transformation of chemical energy into electrical energy consists of the decomposition of methanol molecules, losing their hydrogen's to produce electricity, carbon dioxide and pure water [2]. Pirtskhalava et al. (1962) studied the influence of the acid anions Cl⁻, Br⁻, I⁻, HSO₄⁻ and H₂PO₄⁻ adsorbed on the electro-oxidation of methanol on platinum electrodes. Thereafter, sulfuric acid was used as an acid medium in the working electrolyte [3]; subsequently the cyclic voltammetry process was applied by Breiter (1962) in the MOR in acid medium [4]. Several transition metals have been tested in MOR, Breiter in 1963 analyzed the Pt, Ir, Rh and Au in the potential window (0.07-1.4) V while the Pd in the range (0.2-1.0) V using HClO₄ as medium acid, concluding that in these potential windows, only Pt and Pd oxidize methanol [5]. In 1967, the first systematic study on the mechanism of electro-oxidation of methanol in an acid medium (using H₂SO₄) was published mentioning the intermediate species methoxy CH₂OH, formaldehyde CHOH, aldehyde CHO, carbon monoxide CO and carbon dioxide CO₂ [6-8]. Later Bagotsky discovered that formic acid HCOOH was generated during the MOR [9]. In 1979 Hampson and Willars [10] established methanol as a particularly promising compound for its use in a low temperature, aqueous electrolyte fuel cell, proposing the following reaction model:



Several aspects have been discovered around the mechanism of methanol electro-oxidation in acid medium in line with advances in the science and technology of measurement equipment used with new theories and techniques of characterization of materials such as: X-ray photoelectron spectroscopy [11], in-situ IR studies [12], molecular orbital theory [13], relativistic density-functional theory [14], electrochemically

modulated infrared spectroscopy [15], electro-chemical cell with ultra high vacuum system coupled [16], in-situ X-ray absorption spectroscopy [17] and Electrochemical Mass Spectrometry [18]. Fig. 1 shows the typical CV profile of methanol electro-oxidation process in acid medium ($\text{CH}_3\text{OH} + \text{H}_2\text{SO}_4$) in potential window -0.2 V to 1.0 V using Pt as active phase.

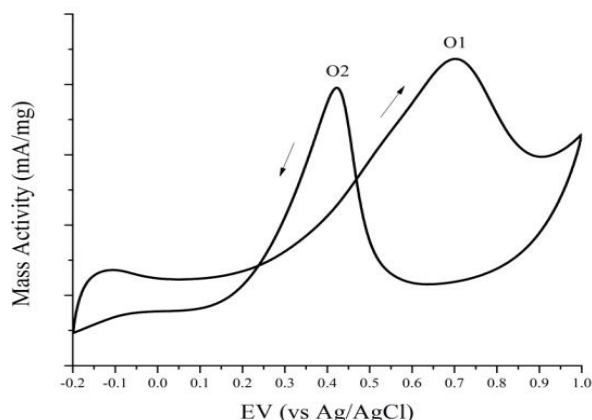


Fig. 1. Typical Voltammogram of the MOR in acid medium (0.5M H_2SO_4 +1.0M CH_3OH)

In these CV profile two oxidation peaks O1 and O2 can be observed attributed mainly to incomplete oxidation of methanol and oxidation of carbonaceous intermediates species formed during forward scan [19].

II. MATERIALS AND METHODS

2.1 Chemicals

Methanol (CH_4O , 99.9%) was supplied by J.T. Baker. Pluronic P123 (non-ionic triblock copolymer, $\text{EO}_{20}\text{PO}_{70}\text{O}_{20}$), tetraethoxysilane ($\text{Si}(\text{OC}_2\text{H}_5)_4$, 98%), platinum (II) acetylacetonate ($\text{Pt}(\text{C}_5\text{H}_7\text{O}_2)_2$, 97%), cobalt(II) nitrate hexahydrate ($\text{Co}(\text{NO}_3)_2 \cdot 6\text{H}_2\text{O}$, 99.99%), Nickel (II) nitrate hexahydrate ($\text{Ni}(\text{NO}_3)_2 \cdot 6\text{H}_2\text{O}$, 99.999%), iron (III) nitrate nonahydrate ($\text{Fe}(\text{NO}_3)_3 \cdot 9\text{H}_2\text{O}$, 99.99%), nafion 117 solution, platinum on graphitized carbon (Pt/XC-72; 10 wt% Pt loading) were obtained from Sigma-Aldrich. Sulfuric acid (H_2SO_4 , 98%), sodium hydroxide (NaOH , 99.9%), ammonium hydroxide (NH_4OH , 30% as NH_3), hydrochloric acid (HCl , 37%), nitric acid (HNO_3 , 70%), acetone ($\text{C}_3\text{H}_6\text{O}$, 99.5%), ethyl alcohol ($\text{C}_2\text{H}_6\text{O}$, 99.7%) and citric acid ($\text{C}_6\text{H}_8\text{O}_7$, 99.5%) were supplied by Fermont. Refined sugar was obtained by Del Marques. Ultrapure water ($15 \text{ M}\Omega\text{cm}^{-1}$) was generated by ELGA Purelab Option station.

2.2 Synthesis and oxidation of MNC

The MNC sample was synthesized via nanocasting process with anhydrous pyrolysis at $800 \text{ }^\circ\text{C}$ using SBA-15 as hard template according with the established in a previous work [20]. In brief, 20.0 g Pluronic P-123 were dissolved in 140 mL ultrapure water and 600 mL of 0.6 M hydrochloric acid by stirring at room temperature for 5 h, afterwards, 43 mL of tetraethoxysilane (TEOS) were added dropwise and the mixture was stirred (700 rpm) at $45 \text{ }^\circ\text{C}$ for 24 h. After, the mixture was aged in oven at $90 \text{ }^\circ\text{C}$ for 24 h. The white powder was obtained through filtration, washing and drying under vacuum. Finally, the sample was calcined at $550 \text{ }^\circ\text{C}$ for 6 h under air to obtain the silica template. On the other hand, 10 g of refined sugar and 10 g of SBA-15 were dissolved in 50 mL of ultrapure water by stirring at room temperature for 30 min, during this time 0.5 mL of sulfuric acid was added. The mixture was heated in an oven at $100 \text{ }^\circ\text{C}$ for 6 h, and subsequently $160 \text{ }^\circ\text{C}$ for another 6 h. The silica sample, containing partially polymerized and carbonized refined sugar, was carbonized in a quartz furnace at $900 \text{ }^\circ\text{C}$ for 1 h under N_2 flow. After pyrolysis, the silica template was removed under vigorous stirring using the solution 1M NaOH at the room temperature for 2 h. Afterwards the black powder was obtained through filtration, washing with ultrapure water and drying in an oven at $80 \text{ }^\circ\text{C}$ for 12 h. The final product was denoted as MNC. The functionalization or oxidation process was carried out with a solution 1M $\text{HNO}_3 + 1\text{M } \text{H}_2\text{SO}_4$ by refluxing MNC at $110 \text{ }^\circ\text{C}$ by 5 h in order to generate surface oxides such as carboxylic ($-\text{COOH}$), carbonyl ($-\text{C}=\text{O}$), and hydroxyl ($-\text{C}-\text{OH}$) groups on the support surface. Afterward, filtered and washed with excess ultrapure water, and dried in N_2 at $150 \text{ }^\circ\text{C}$ in a tubular furnace by 2 h [21-22].

2.3 Synthesis of Pt/MNC, Co/MNC, Fe/MNC and Ni/MNC

The Pt/MNC, Co/MNC, Fe/MNC and Ni/MNC samples (with 10 wt% metal loading) were synthesized by a wet incipient wetness impregnation method and chemical reduction route. For Pt/MNC, 0.2563 mM

$\text{Pt}(\text{C}_5\text{H}_7\text{O}_2)_2$ were dissolved in 20 mL of acetone and simultaneously 0.45 g of MNC (oxidized) were dissolved in 30 mL of ultrapure water. Both are mixed under mechanical stirring at room temperature until a homogeneous mixture. Then the dispersion was sonicated for 30 min, afterwards, 0.333 mM $\text{C}_6\text{H}_8\text{O}_7$ was added to the solution in mechanical stirring for 5 h at room temperature under Ar- H_2 (90%-10%) atmosphere in order to remove isolate oxygen. After reaction, the obtained products were filtrated, washed with ultrapure water and then vacuum dried. The impregnated carbon sample was heated in a quartz furnace a flowing Ar- H_2 environment while increasing temperature from the room temperature to 250 °C over 1 h then to 400 °C over 2 h. For Co/MNC, 0.8485 mM $(\text{Co}(\text{NO}_3)_2 \cdot 6\text{H}_2\text{O})$ were dissolved in 40 mL of ultrapure water 0.4 mL NH_4OH were added to the solution and mechanically stirred until a homogeneous mixture. Afterwards, the dispersion was sonicated for 30 min in where 1.103 mM $\text{C}_6\text{H}_8\text{O}_7$ were added. Then the mixture was mechanical stirring for 5 h at room temperature under Ar- H_2 (90%-10%). After reaction, the obtained products were filtrated, washed with ultrapure water and then vacuum dried. The impregnated carbon sample was heated a flowing Ar- H_2 atmosphere while increasing temperature from the room temperature to 250 °C over 1 h then to 400 °C over 2 h. Similar procedure were applied for Fe/MNC and Ni/MNC with appropriate amounts of salts precursors of both Fe and Ni respectively [23-25].

2.4 Characterization of Materials

In order to determine the textural properties of SBA-15 and MNC, they were analyzed on a Quantachrome model Autosorb-iQ ASIQA0000-2 at 77K. The specific surface area (ABET) by the Brunauer–Emmet–Teller (BET) method was determined. Pore size distributions (PSDs) were obtained from the adsorption branch of the nitrogen isotherm using the Barrett–Joyner–Halenda equation. The FTIR spectroscopy study of hard template and catalytic support has been realized in mid-IR region ($4000\text{-}380\text{ cm}^{-1}$) with a spectrophotometer Perkin Elmer model Spectrum100. To determine the binding energies associated with ionic or covalent bonds between the atoms, the samples were analyzed with a high-resolution X-ray photoelectron spectroscopy (XPS-HR) equipment from SPECS with Al anode (1486.71 eV) as a source of X-rays. The small angle XRD patterns of SBA-15 and MNC were obtained with a Siemens D500 X-ray diffractometer and XRD patterns were collected on a Bruker D8 Advance X-ray diffractometer with Cu $K\alpha$ radiation. The Raman measurements were carried out using a Bruker model Raman-Senterra spectrometer with Olympus BX microscope and Ar laser (785 nm). Field emission scanning electron microscopy (FESEM) images and the X-ray energy dispersion spectroscopy (EDS) spectra were obtained using the JEOL JSM-7600F scanning electron microscope with an EDS detector coupled from Oxford Instruments operating at 30 keV in GB-LOW mode [26].

2.5 Electrochemical measurements

The performance of Pt/MNC, Co/MNC, Fe/MNC, Ni/MNC and commercial catalysts (Pt/XC-72) for room temperature methanol oxidation reaction was measured in an electrochemical work station BASi-epsilon (potentiostat/galvanostat). A conventional three-electrode cell with glassy carbon (GC) as working electrode, Pt wire as counter electrode and Ag/AgCl (0.1M KCl) as reference electrode were used for the cyclic voltammetry tests. A glassy carbon electrode (3 mm) was sequentially polished with 0.05 μm Al_2O_3 and then washed. The catalyst ink was prepared by ultrasonically dispersing 10 mg catalyst in 1 mL of ethanol and 60 μL Nafion/water (25% Nafion) for 1 h. 10 μL of the dispersion was transferred on the GC and then dried in the air for 45 min [27]. The electrolyte solution for methanol oxidation reaction consists of 1 M CH_3OH and 0.5 M H_2SO_4 and the CV's were recorded at a scanning rate of 20 mV/s and 10 cycles for each [28].

III. RESULTS AND DISCUSSION

3.1. BET analysis

The SBA-15 and MNC samples were characterized by physisorption of N_2 at 77 K. Fig. 2 shows the isotherms of hard template and MNC after functionalization process.

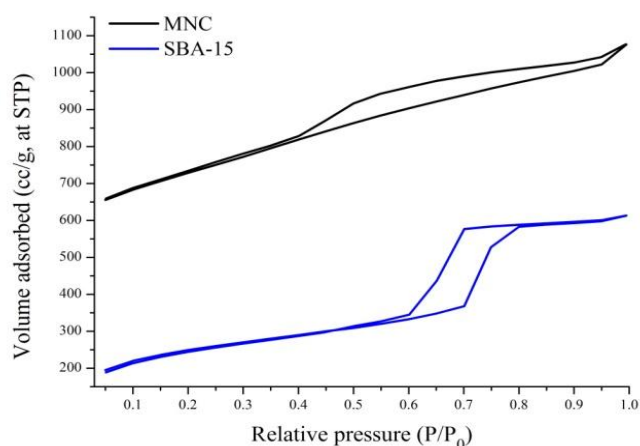


Fig. 2. N₂ adsorptions isotherms of MNC and SBA-15

It can be seen for both samples type IV isotherms in which SBA-15 shows an H1 hysteresis loop while MNC shows a type IV hysteresis loop [29]. According to BJH analysis, the pore size distribution for SBA-15 and MNC are centered at approximately 6.5 and 3.8 nm, respectively. The BET method applied shows that the A_{BET} for SBA-15 and MNC were 832 m²/g and 995 m²/g, respectively. It is notable that the A_{BET} of MNC was less than that obtained before the functionalization process (1150 m²/g) due to the oxygenated groups formed on the pore surface. This analysis reveals the mesostructure of SBA-15 and MNC.

3.2. FTIR analysis

In order to observe the evolution of the synthesis of MNC as well as to confirm the presence of surface oxygenated groups, a FTIR in the mid-IR region (4000–380 cm⁻¹) was applied. Figure 3 shows the FTIR spectra of SBA-15 and MNC after the functionalization process. For SBA-15, three absorption bands at approximately 1047, 967, and 807 cm⁻¹ correspond to the stretch vibration of the Si-O-Si group, a strong band at approximately 486 cm⁻¹ corresponding to the Si-O group, and a weak and broad band at approximately 3560 cm⁻¹ attributed to the stretching vibrations of the surface silanol groups (Si-OH) and the remaining adsorbed water molecules in the O-H bond.

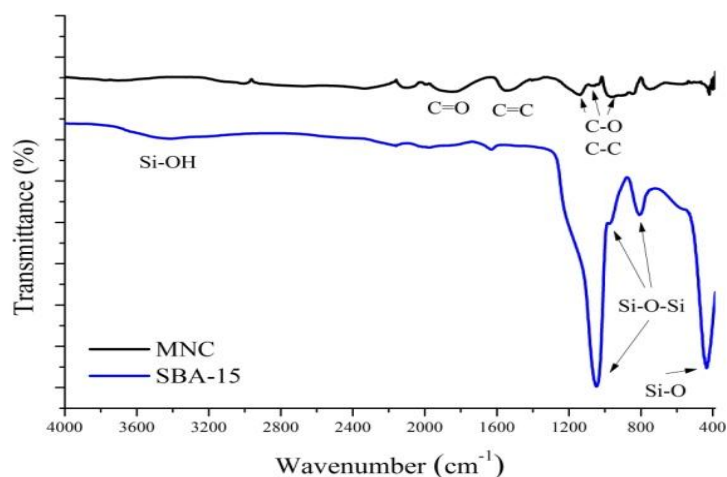


Fig. 3. FTIR spectra of MNC and SBA-15

The FTIR profile of MNC (after both oxidation and silica removal processes) shows an absorption band at approximately 1832 cm⁻¹ corresponding to the stretch vibration of a double bond in C=O, typical of carboxylic groups, a band at approximately 1538 cm⁻¹ corresponding to the stretch vibration of a double bond in C=C, and three weak and broad bands at approximately 1399, 1060, and 971 cm⁻¹ attributed to the stretching vibrations in the C-C bond of the carbon network and C-O in oxygenated groups [30]. The disappearance of the bands corresponding to the silanol group demonstrates the efficiency of the silica removal process.

3.3. XPS analysis

Figure 4 shows the X-ray photoelectron spectra of the oxidation states and spectral lines of metallic species Pt, Co, Ni and Fe into the Pt/MNC, Co/MNC, Ni/MNC and Fe/MNC.

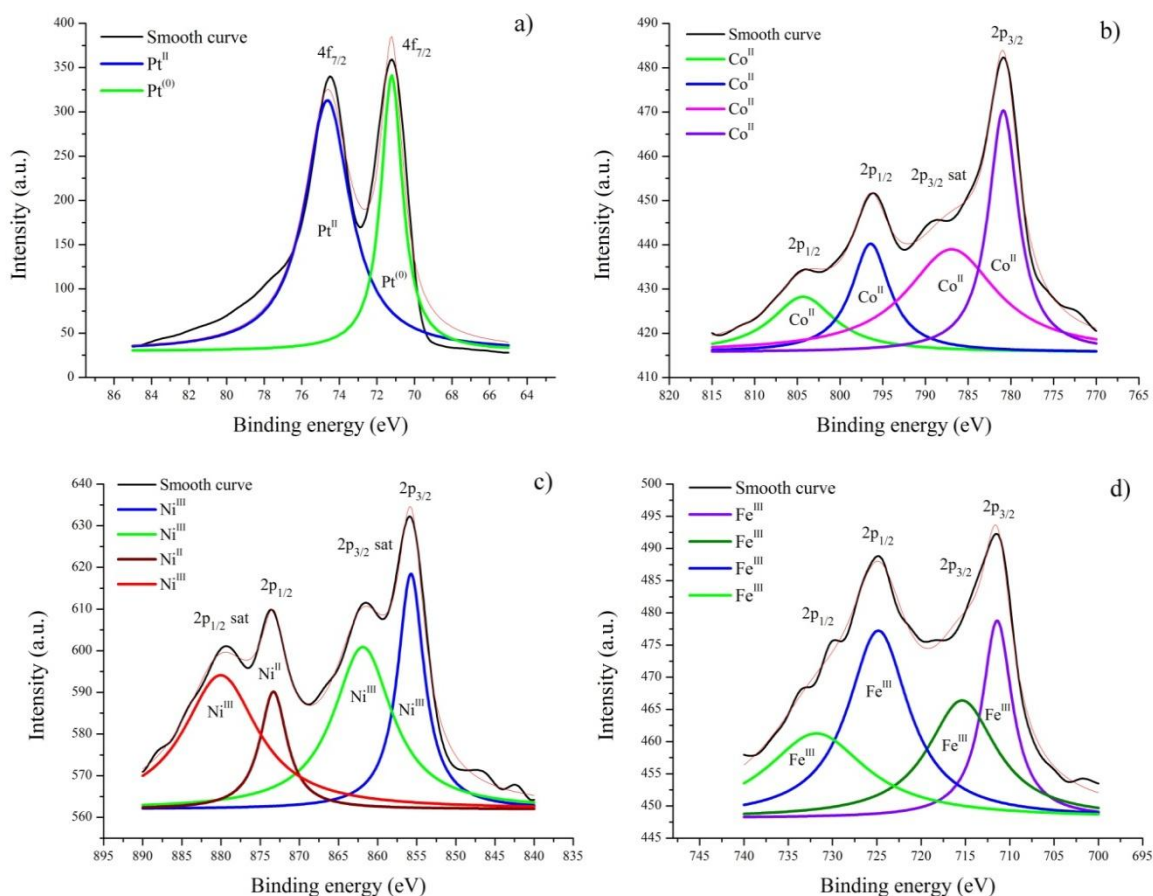


Fig. 4. XPS spectra of the metallic species a) Pt; b) Co; c) Ni and d) Fe

The deconvolution of XPS spectrum of Pt (Fig. 4a) reveals three peaks attributed to the element states Pt⁽⁰⁾ (71.2 eV, 4f_{7/2}) and Pt^(II) (74.6 eV, 4f_{7/2}) corresponding to Pt and PtO respectively [31-32]; for the Co, four peaks appear (Fig. 4b) attributed to oxidation state Co^(II) [(780.5 eV, 2p_{3/2}), (787.5 eV, 2p_{3/2} sat), (796.4 eV, 2p_{1/2}) and (803.7 eV, 2p_{1/2})] that correspond to CoO and Co(OH)₂ [33-34]; the XPS spectrum of Ni shows four peaks (Fig. 4c) that corresponding to oxidation state Ni^(II) [(861.7 eV, 2p_{3/2} sat)] and Ni^(III) [(855.6 eV, 2p_{3/2}), (873.1 eV, 2p_{1/2}) and (879.7 eV, 2p_{1/2} sat)] attributed to compounds such as NiOOH and Ni(OH)₂ [35-36]; finally the deconvolution of Fe XPS spectrum (Fig. 4d) shows four peaks attributed to Fe^(III) [(711.4 eV, 2p_{3/2}), (715.4 eV, 2p_{3/2}), (724.3 eV, 2p_{1/2}) and (731.8 eV, 2p_{1/2})] that correspond to the compounds FeOOH and probably Fe₂O₃ [37-39]. The possible existence of NiOOH, FeOOH, Co(OH)₂, Ni(OH)₂, PtO and Fe₂O₃ it can be explain by the presence of the both oxygen and hydrogen in the citric acid structure and the water used in the synthesis processes.

3.4. XRD analysis

In order to analyze the mesostructure of the SBA-15 and MNC samples, X-ray diffraction technique in the small angle range 0.5-6° in 2θ scale was applied. Fig. 5 shows small-angle patterns of these samples. For SBA-15, it can be observe three diffraction peaks at around 1.01, 1.67 and 1.9° which correspond to diffraction planes (100), (110) and (200) respectively, attributed to a highly ordered hexagonal (p6mm) mesostructure and to the periodicity of the pores array [40]. Is evident that for MNC the planes (110) and (200) not appear, suggesting that the links between carbon nanofibers (or carbon nanopipes) are loosed, due to a higher temperature used in the anhydrous pyrolysis process (900 °C), however the presence of plane (100), indicate that the carbon nanofibers are kept join maybe due to thin layers of graphene that covers them [41].

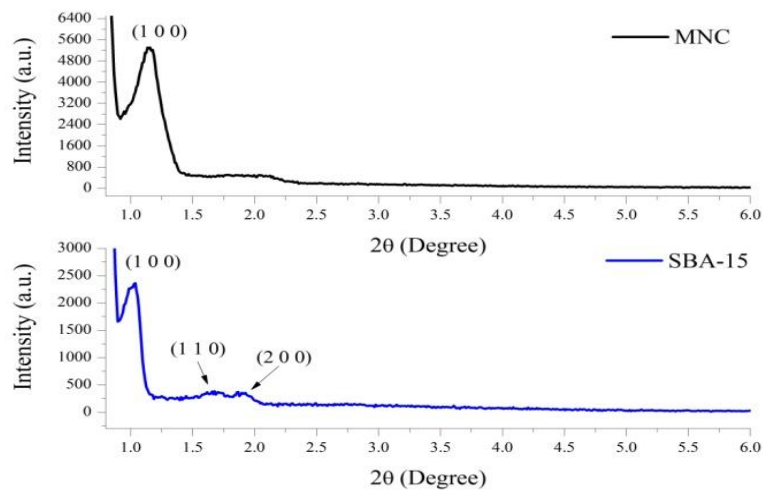


Fig. 5. Small-angle XRD patterns of SBA-15 and MNC

In order to obtain more information about the MNC structure, wide-angle X-ray diffraction technique was applied in the range 10-90° in 2θ scale. Figure 6 shows the XRD pattern of MNC. For MNC, one strong but broad peak at around 23.7° and two weak peaks at around 43° and 79.1° which correspond to the planes (002), (10) and (11) respectively; a shift of (002) reflection toward lower diffraction angles (in comparison with graphite at $2\theta = 26.3^\circ$) is observed [42].

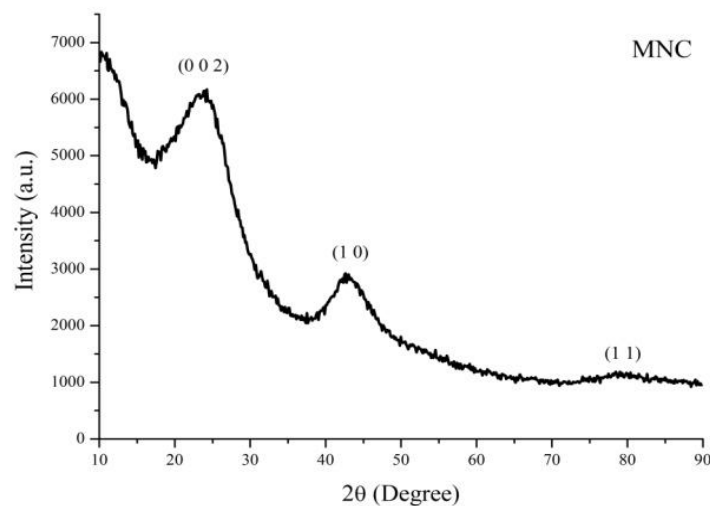


Fig. 6. Wide-angle XRD profile of MNC

The existence and the shift of (002) reflection is an indicative that the MNC sample have an intermediate structure between amorphous coal and graphite, commonly called turbostratic carbon [43-44] which suggesting that the MNC consist in graphene sheets with large curvature, carbon nanofibers and carbon nanpipes with certain graphitization degree. On the other hand, Fig. 7 shows XRD pattern of Pt/MNC, Co/MNC, Ni/MNC and Fe/MNC in wide angle in the range 10-90° in 2θ scale.

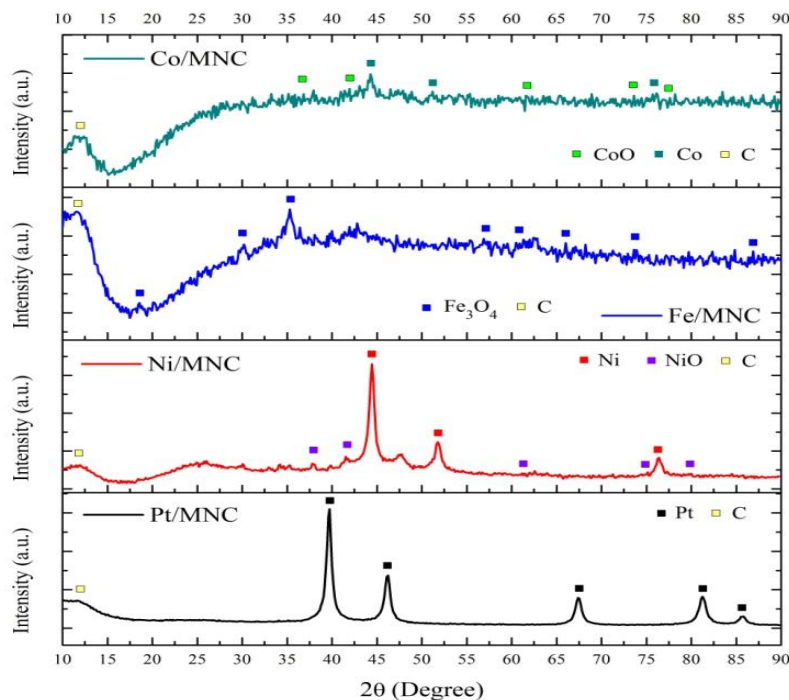


Fig. 7. XRD patterns of Co/MNC, Fe/MNC, Ni/MNC and Pt/MNC.

For the cobalt in Co/MNC, three diffraction peaks are detected at around 44.3, 51.6 and 75.7° corresponding to the planes (111), (200) and (220) of face centered cubic (fcc) of Co (JCPDS-015-0806) furthermore, five peaks at around 36.8, 42.4, 61.9, 73.6 and 77.6° attributed to the planes (111), (200), (220), (311) and (222) of the fcc crystalline structure of CoO (JCPDS-048-1719). In the XRD pattern of Fe/MNC, seven diffraction peaks are detected at around 18.6, 30.2, 35.3, 56.6, 62.4, 66.7, 66.7 and 73.9° attributed to the planes (111), (200), (311), (333), (440), (442) and (533) of the fcc crystalline structure of Fe₃O₄ (JCPDS-082-1533). For the nickel in Ni/MNC, three diffraction peaks are detected at around 44.4, 51.7 and 76.4° corresponding to the planes (111), (200) and (220) of the fcc structure of Ni (JCPDS-065-8665) furthermore, five peaks at around 37.8, 43.2, 62, 75.1 and 78.9° attributed to the planes (111), (200), (220), (311) and (222) of the fcc crystalline structure of NiO (JCPDS-004-0835). For platinum in Pt/MNC, the typical five diffraction peaks are detected at around 39.7, 46.2, 67.4, 81.2 and 85.8° attributed to the planes (111), (200), (220), (311) and (222) of the fcc crystalline structure of Pt (JCPDS-071-3756). In all materials one diffraction peak at around 11.77° corresponding to (002) reflection of C is detected. The average particle size of Pt/MNC, Co/MNC, Ni/MNC and Fe/MNC was roughly calculated according to Debye-Scherrer Equation [45]:

$$D_{\text{XRD}} = \frac{0.9\lambda}{\beta_{2\theta} \cos(\theta)} \quad (2)$$

where, D_{XRD} is the average particle size, λ is the X-ray wave-length (0.15406 nm), $\beta_{2\theta}$ is the full width at half maximum, and θ is the angle at peak maximum. The estimated values of crystallite size shows in Table 1.

Table 1. Estimated crystallite size values of Pt/MNC, Co/MNC, Ni/MNC and Fe/MNC

Sample	D_{XRD} (nm)
Pt/MNC	15.6
Co/MNC	12.2
Ni/MNC	18.3
Fe/MNC	9.7

3.5. Raman spectroscopy

Raman spectroscopy is one of the most used techniques to analyze the vibrational behaviour of both sp^2 and sp^3 hybridizations in carbon materials. The Raman spectra of the most carbon materials show two main bands: a G band at around 1575 cm^{-1} associated with the E_{2g} phonon at the Γ point in the first Brillouin Zone of graphite and D band at around 1360 cm^{-1} related with disorder in carbon network attributed to a decrease in symmetry near microcrystallite edges. The intensity ratio I_D/I_G is commonly used to measure the disorder degree of carbon structures [46-47]. Fig. 8a shows the Raman spectrum of MNN before functionalization process in

which it can see the G band at around 1598 cm^{-1} and D band at around 1356 cm^{-1} ; the ratio I_D/I_G was 0.86 suggesting certain disorder degree in the carbon hexagonal network and confirming the graphitization degree achieved by high temperature in the anhydrous pyrolysis process ($900\text{ }^\circ\text{C}$).

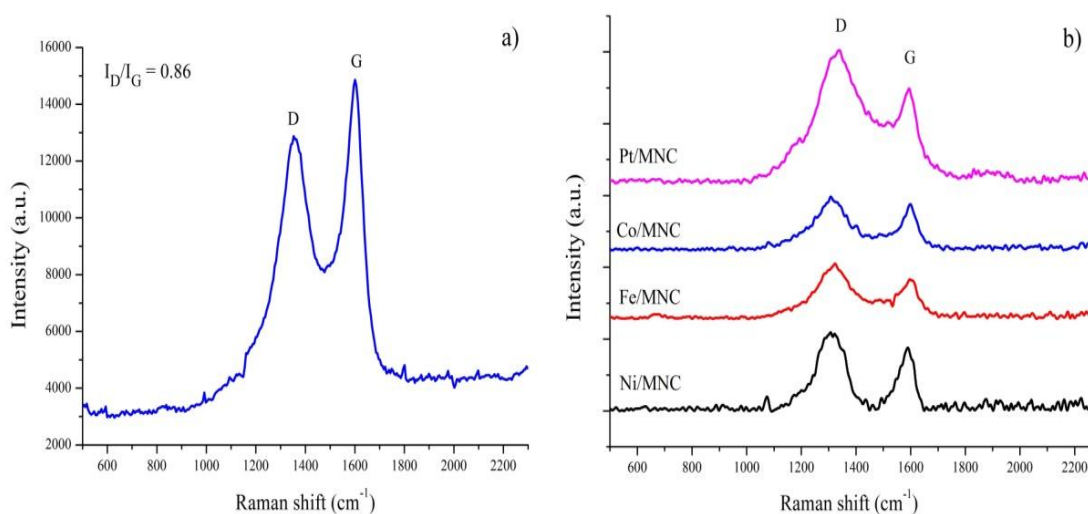


Figure 8: Raman spectra of a) MNC before oxidation process and b) Pt/MNC, Co/MNC, Ni/MNC and Fe/MNC.

The Raman spectra of Pt/MNC, Co/MNC, Ni/MNC and Fe/MNC in Fig. 8b are illustrated, in which for all cases a G band at around 1594 cm^{-1} is detected as well as a D band at around 1310 cm^{-1} of higher intensity compared to its corresponding G band. In these order, the I_D/I_G ratio were 1.11, 1.03, 1.24 and 1.12; the increase of D band of these materials with respect to D band of MNC can be explain by the presence of oxygenated groups and the strong metal bond on surface of MNC which produce an alteration in the vibrational behaviour of the carbon hexagonal network [48].

3.6. STEM and EDS analysis

In order to determine both morphology and microstructure of the samples, the scanning electron microscopy technique was applied. The SEM images of SBA-15 and MNC in Fig. 9 are illustrated.

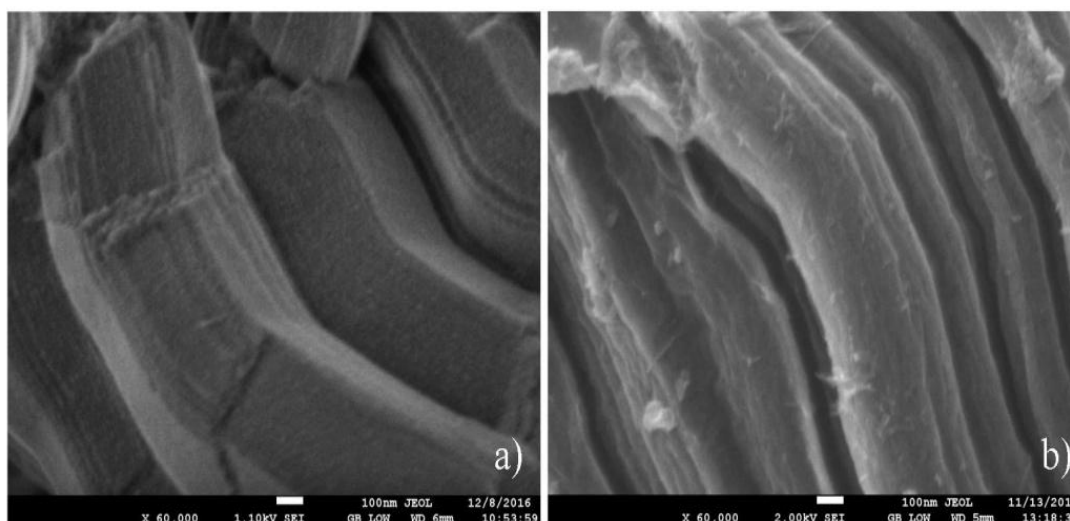


Fig. 9. SEM images of a) SBA-15 and b) MNC

The SEM analysis of SBA-15 (Fig. 9a) reveals that has a rope-like morphology whose pseudo-cylinder elements are approximately 400 nm in diameter, while that for MNC this same morphology is retained due to nanocasting process. A detailed analysis reveals that MNC has thin graphene layers overlaying carbon nanofibers with 7 nm in diameter (Fig. 9b). The SEM images of Pt/MNC, Co/MNC, Ni/MNC and Fe/MNC at

60,000 X of magnification and 2.0 keV in GB-LOW mode (Fig. 10) shows metallic nanoparticles highly dispersed on MNC with spherical and irregularly shaped morphologies and whose diameter oscillated in the range (8-20) nm.

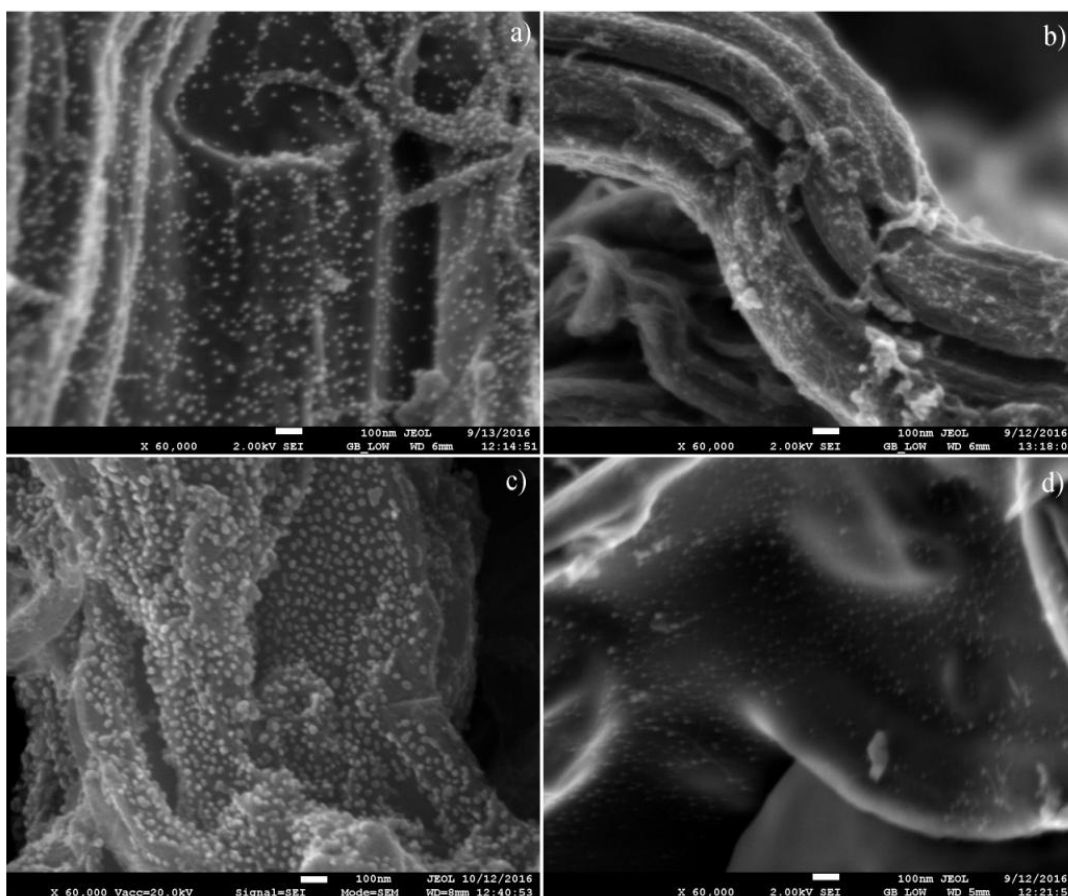


Fig. 10. SEM images of a) Pt/MNC; b) Co/MNC; c) Ni/MNC and d) Fe/MNC.

To determine the average chemical composition of samples (Table 2), energy dispersive X-ray spectroscopy was applied at 20 keV, whose EDS spectra in Figure 11 are illustrated. For SBA-15 it can see the presence of Si and O typical components of the mesoporous silica materials while for MNC (after functionalization process) demonstrate the existence of oxygen in hydroxyl, carboxyl and carbonyl groups; these results is in accordance with FTIR analysis. On the other hand, for Pt/MNC, Co/MNC, Ni/MNC and Fe/MNC their EDS spectrum shows the corresponding elements Pt, Co, Ni and Fe.

Table 2. Average elemental composition of all samples

Sample	EDS wt %						
	C	Si	O	Pt	Co	Ni	Fe
SBA-15	-	61.07	38.93	-	-	-	-
MNC	85.44	0.05	14.51	-	-	-	-
Pt/MNC	75.76	0.01	13.37	10.86	-	-	-
Co/MNC	76.94	0.01	13.40	-	9.65	-	-
Ni/MNC	75.46	0.05	14.26	-	-	10.23	-
Fe/MNC	74.66	0.08	14.25	-	-	-	11.01

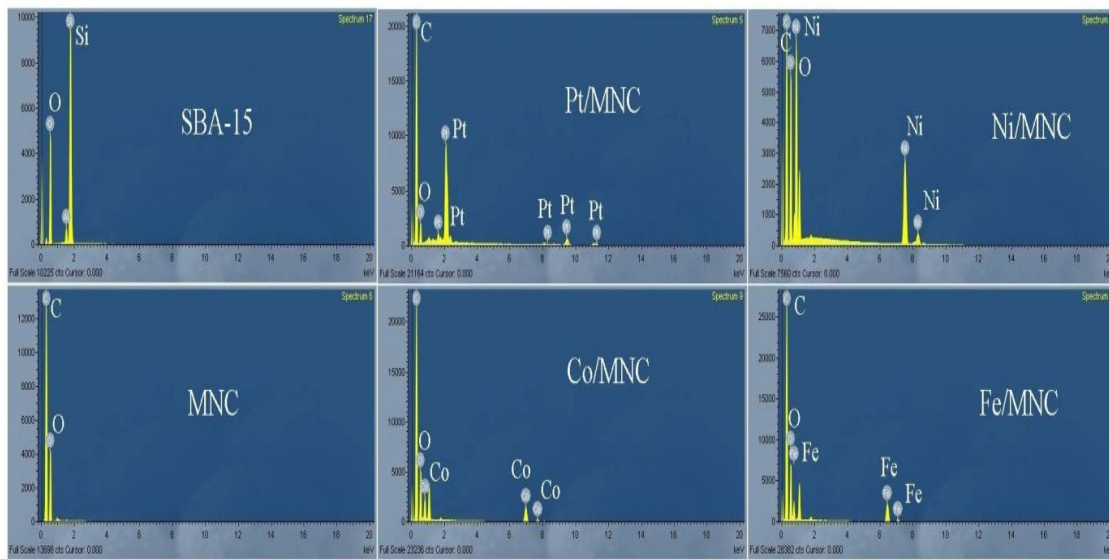


Figure 11: EDS spectra of all samples.

3.6. Electrochemical measurements

The cyclic voltammetry technique was applied using as electrolyte 0.5 M H₂SO₄ + 1.0 M CH₃OH, 10 cycles and a potential window of -2.0 V to 1.0 V; the density current was normalized to metal loading. Figure 12 shows the CV profiles of Co/MNC, Ni/MNC and Fe/MNC in acid medium, which present two current peaks corresponding to oxidation-reduction electro-chemical processes and cannot be attributed to methanol oxidation reaction as can be seen in Fig. 1.

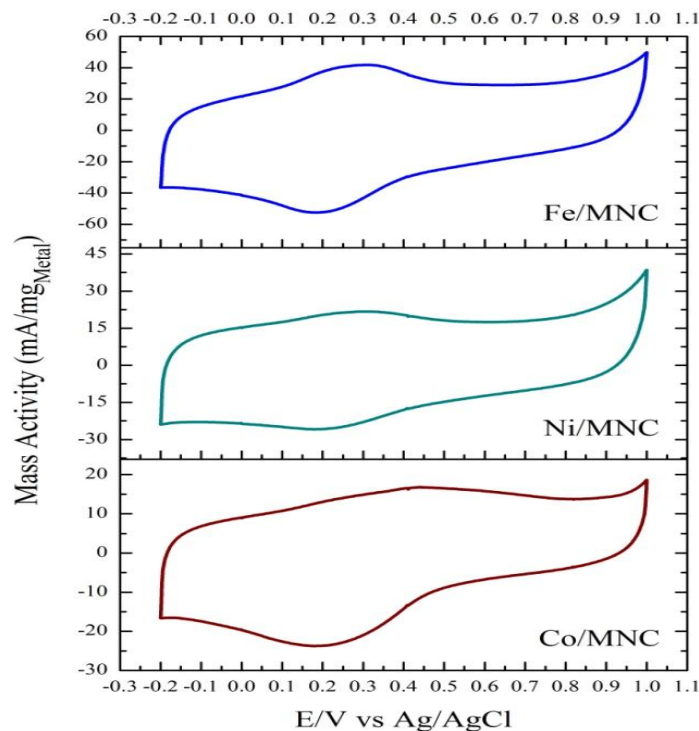
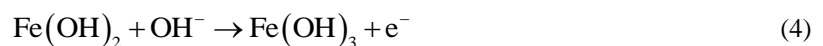
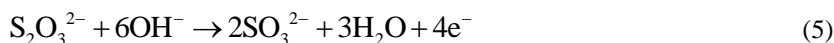


Fig. 12. CV profiles of Co/MNC, Ni/MNC and Fe/MNC in 0.5 M H₂SO₄ + 1.0 M CH₃OH

The oxidation-reduction semi-reactions can be the following [49]:





In addition, these voltammograms show the tendency to a square shape, which suggests that these materials possess capacitive ability given the presence of a double layer at the electrode-electrolyte interface [50]. On the other hand, the CV profile of Pt/MNC (Fig. 13) shows the two typical oxidation peaks of the methanol oxidation reaction such like show Fig. 1, and in contrast to the voltammogram of the commercial catalyst Pt/XC-72, the Pt/MNC sample exhibit a best tolerance towards accumulated carbon intermediate species; this tolerance commonly is measured trough I_{CO} index that to related the current at forward scan and current at backward scan. Is notable that Pt/MNC has a best performance of both current density generation and I_{CO} index with respect to Pt/XC-72 due mainly to a greater ability of Pt to adsorb hydroxyl groups and the synergetic effect with MNC for oxidize the accumulated carbonaceous species [11,51].

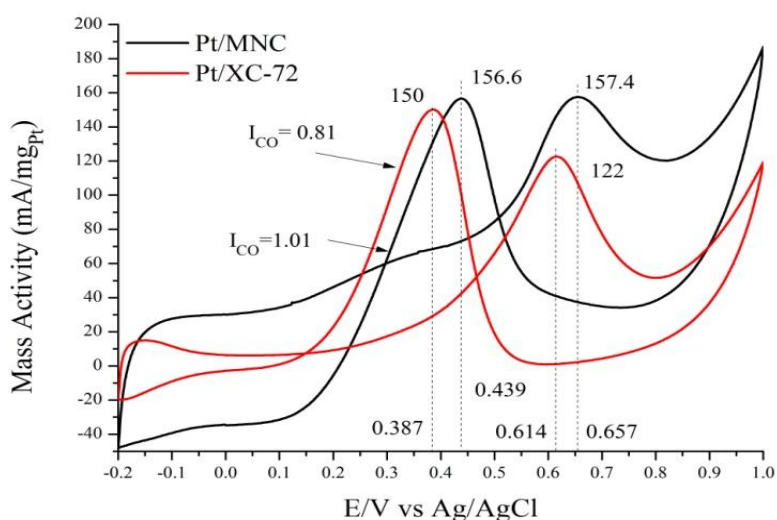


Fig. 13. Cyclic voltammograms of methanol electro-oxidation on Pt/MNC and Pt/XC-72

IV. CONCLUSION

According with the CV results Pt/MNC catalyst exhibit a best performance in methanol oxidation reaction that commercial catalyst Pt/XC-72 with 10% wt loading whereas the materials Co/MNC, Ni/MNC and Fe/MNC have a tendency towards capacitive abilities and they did not have catalytic activity in methanol oxidation process in the potential window -2.0 V to 1.0 V.

V. ACKNOWLEDGEMENTS

David Macias Ferrer gratefully acknowledges a scholarship from to National Council for Science and Technology (387542/269139) and would like to thanks for financial assistance from the National Technological Institute of Mexico/ Technological Institute of Cd. Madero (5261.14-P) Center for Research in Secondary Petrochemistry, Bays Avenue, Tecnia Industrial Park, Altamira, Tamaulipas, México.

REFERENCES

- [1]. R. Schreiner, Anodische Oxydation der Essigsäure in Schwefelsaurer Lösung, Zeitschrift für Elektrochemie und Angewandte Physikalische Chemie, 36, 1930, 953-1040.
- [2]. H. Liu, J. Zhang, Electrocatalysis of Direct Methanol Fuel Cells From Fundamentals to Applications (Darmstadt, Germany: WILEY-VCH Verlag GmbH & Co. KGaA, 2009).
- [3]. D.N. Pirtskhalava, Y.V. Vasiliev, V.S. Bagotzky, Influence of Anions of the Electrooxidation of Methanol on Platinum Electrode J. Acad. Sci. USSR, 1962, 1425-1430.
- [4]. M.W. Breiter, Double Layer Capacity and Methanol Coverage on Platinum in Perchloric Acid Solution, Electrochimica Acta, 7, 1962, 533-542.
- [5]. M.W. Breiter, Comparative Voltammetric Study of Methanol Oxidation and Adsorption on Noble Metal Electrodes in Perchloric Acid Solutions, Electrochimica Acta, 8, 1963, 973-983.
- [6]. V.S. Bagotzky, Y.V. Vasiliev, Absorption of Organic Substances on Platinum Electrodes, Electrochimica Acta, 11, 1966, 1439-1461.
- [7]. V.S. Bagotzky, Y.V. Vasiliev, Mechanism of Electro-Oxidation of Methanol on the Platinum Electrode, Electrochimica Acta, 12, 1967, 1323-1343.

- [8]. V.S. Bagotzky, Y.V. Vasiliev, O.A. Khazova, S.S. Sedova, Adsorption and Anodic Oxidation of Methanol on Iridium and Rhodium Electrodes, *Electrochimica Acta*, 16, 1971, 913-938.
- [9]. V.S. Bagotzky, Y.V. Vasiliev, O.A. Khazova, Generalized Scheme of Chemisorption, Electrooxidation and Electroreduction of Simple Organic Compounds on Platinum Group Metals, *J. Electroanal. Chem.*, 81, 1977, 229-238.
- [10]. N.A. Hampson, J.M. Willars, B.D. McNicol, The Methanol-Air Fuel Cell: A Selective Review of Methanol Oxidation Mechanisms at Platinum Electrodes in Acid Electrolytes, *J. Power Source*, 4, 1979, 191-201.
- [11]. J.B. Goodenough, A. Hamnett, B.J. Kennedy, R. Manoharan, Methanol Oxidation on Unsupported and Carbon Supported Pt + Ru Anodes, *J. Electroanal. Chem.*, 240, 1988, 133-145.
- [12]. T. Iwasita, Vielstich, New In-Situ IR Results on Adsorption and Oxidation of Methanol on Platinum in Acidic Solution, *J. Electroanal. Chem.*, 250, 1988, 451-456.
- [13]. A.B. Anderson, E. Grantscharova, Catalytic Effect of Ruthenium in Ruthenium-Platinum Alloys on the Electrooxidation of Methanol. *Molecular Orbital Theory*, *J. Phys. Chem.*, 99, 1995, 9149-9154.
- [14]. Y. Ishikawa, M.S. Liao, C.R. Cabrera, Oxidation of Methanol on Platinum, Ruthenium and Mixed Pt-M Metals (M=Ru, Sn): A Theoretical Study, *Surface Science.*, 463, 2000, 66-80.
- [15]. T. Iwasita, F.C. In Situ Infrared Spectroscopy at Electrochemical Interfaces, *Nart, Prog. Surf. Sci.*, 55(4), 1997, 271-340.
- [16]. E.A. Batista, H. Hoster, T. Iwasita, Analysis of FTIRS data and thermal effects during methanol oxidation on UHV-cleaned PtRu alloys, *J. Electroanal. Chem.*, 554-555, (2003) 265-271.
- [17]. W.L. Holstein, H.D. Rosenfeld, In-Situ X-ray Absorption Spectroscopy Study of Pt and Ru Chemistry during Methanol Electrooxidation, *J. Phys. Chem. B.*, 109, 2005, 2176-2186.
- [18]. T.H.M. Housmans, A.H. Wonders, M.T.M. Koper, Structure Sensitivity of Methanol Electrooxidation Pathways on Platinum: An On-Line Electrochemical Mass Spectrometry Study, *J. Phys. Chem. B.*, 110, 2006, 10021-10031.
- [19]. R. Manoharan, J.B. Goodenough, Methanol Oxidation in Acid on Ordered NiTi, *J. Mater. Chem.*, 2(8), 1992, 875-887.
- [20]. D. Macias-Ferrer, J.A. Melo-Banda, R. Silva-Rodrigo, U. Páramo-García, J.Y. Verde-Gómez, P. Del-Ángel-Vicente, Synthesis of Micro/nanostructured Carbon from Refined Sugar and its Electrochemical Performance, *Int. J. Electrochem. Sci.*, 13(1), 2018, 708-718.
- [21]. D. Macias-Ferrer, J.A. Melo-Banda, U. Páramo-García, R. Silva-Rodrigo, Nanopartículas de PtNi sobre Carbono Mesoporoso para la Electro-Oxidación de Metanol en Medio Ácido, *Exploratoris. Revista de la Realidad Global.*, 6(2), 2017, 255-262.
- [22]. E. Antolini, Carbon Supports for Low-Temperature Fuel Cell Catalysts, *Applied Catalysis B: Environmental.*, 88, 2009, 1-24.
- [23]. M.S. Saha, R. Li, X. Sun, High Loading and Monodispersed Pt Nanoparticles on Multiwalled Carbon Nanotubes for High Performance Proton Exchange Membrane Fuel Cells, *J. Power Sources.*, 177, 2008, 314-322.
- [24]. K.W. Park, K.S. Ahn, Y.C. Nah, J.H. Choi, Y.E. Sung, Electrocatalytic Enhancement of Methanol Oxidation at Pt-WO_x Nanophase Electrodes and In-Situ Observation of Hydrogen Spillover Using Electrochromism, *J. Phys. Chem. B.*, 107(18), 2003, 4352-4355.
- [25]. A. Santasalo-Aarnio, M. Borghei, I.V. Anoshkin, A.G. Nasibulin, E.I. Kauppinen, V. Ruiz, T. Kallio, Durability of Different Carbon Nanomaterial Supports with PtRu Catalyst in a Direct Methanol Fuel Cell, *Int. J. Hydrogen Energy.*, 37, 2012, 3415-3424.
- [26]. C.R. Brundle, Ch.A. Evans, Sh. Wilson, *Encyclopedia of Materials Characterization: Surfaces, Interfaces, Thin Films*, (UK, Gulf Professional Publishing, 1992).
- [27]. L. Wu, H. Feng, M. Liu, K. Zhang, J. Li, Graphene-based hollow spheres as efficient electrocatalysts for oxygen reduction, *Nanoscale.*, 5, 2013, 10839-10843.
- [28]. W. Xie, F. Zhang, Z. Wang, M. Yang, J. Xia, R. Gui, Y. Xia, Facile preparation of PtPdPt/graphene nanocomposites with ultrahigh electrocatalytic performance for methanol oxidation, *J. Electroanal. Chem.*, 761, 2016, 55-61.
- [29]. K.S.W. Sing, Reporting Physisorption Data for Gas/Solid Systems with Special Reference to the Determination of Surface Area and Porosity, *Pure & Appl. Chem.*, 54, 1982, 2201-2218.
- [30]. N.B. Colthup, Spectra-Structure Correlations in the Infra-Red Region, *J. Opt. Soc. Am.*, 40(6), 1950, 399-400.
- [31]. T.H. Fleisch, G.W. Zaiac, J.O. Schreiner, G.J. Mains, An XPS Study of the UV Photoreduction of Transition and Noble Metal Oxides, *Appl. Surf. Sci.*, 26, 1986, 488-497.
- [32]. J.S. Hammond, N. Winograd, XPS Spectroscopic Study of Potentiostatic and Galvanostatic Oxidation of Pt Electrodes in H₂SO₄ and HClO₄, *J. Electroanal. Chem. Interfacial Electrochem.*, 78, 1977, 55-69.
- [33]. B.J. Tan, K.J. Klabunde, P.M.A. Sherwood, XPS Studies of Solvated Metal Atom Dispersed (SMAD) Catalysts. Evidence for Layered Cobalt-Manganese Particles on Alumina and Silica, *J. Am. Chem. Soc.*, 113, 1991, 855-861.
- [34]. Y. Okamoto, T. Imanaka, S. Teranishi, Surface Structure of CoO-MoO/Al₂O₃ Catalysts Studied by X-ray Photoelectron Spectroscopy, *J. Catal.*, 65, 1980, 448-460.
- [35]. A.N. Mansour, C.A. Melendres, Characterization of Electrochemically Prepared γ -NiOOH by XPS, *Surf. Sci. Spectra.*, 3, 1994, 271-278.
- [36]. A.N. Mansour, Characterization of β -Ni(OH)₂ by XPS, *Surf. Sci. Spectra.*, 3, 1994, 239-246.
- [37]. M. Bououdina, *Handbook of Research on Nanoscience, Nanotechnology, and Advanced Materials*, (NJ, IGI Global, 2014).
- [38]. B.J. Tan, K.J. Klabunde, P.M.A. Sherwood, X-ray Photoelectron Spectroscopy Studies of Solvated Metal Atom Dispersed Catalysts. Monometallic Iron and Bimetallic Iron-Cobalt Particles on Alumina, *Chem. Mater.*, 2, 1990, 186-191.
- [39]. H. Konno, M. Nagayama, X-ray Photoelectron Spectra of Hexavalent Iron, *J. Electron Spectrosc. Relat. Phenom.*, 18, 1980, 341-343.
- [40]. X. Cui, W.C. Zin, W.J. Cho, C.S. Ha, Nonionic Triblock Copolymer Synthesis of SBA-15 above the Isoelectric Point of Silica (pH = 2-5), *Mater. Letters.*, 59(18), 2005, 2257-2261.
- [41]. Y. Seo, K. Kim, Y. Jung, R. Ryoo, Synthesis of Mesoporous Carbons using Silica Templates Impregnated with Mineral Acids, *Microporous Mesoporous Mater.*, 207, 2015, 156-162.
- [42]. Q. Zhang, N. Lin, T. Xu, K. Shen, T. Li, Y. Han, J. Zhou, Y. Qian, Scalable Synthesis of Carbon Stabilized SiO/Graphite Sheets Composite as Anode for High-Performance Li ion Batteries, *RSC Adv.*, 7, 2017, 39762-39766.
- [43]. Z.M. Gao, H.Z. Jin, X.S. Li, Z. Hua, Phase Transformation Mechanism of Graphite-Turbostratic Graphite in the Course of Mechanical Grinding, *Chem. Res. Chinese. Univ.*, 19(2), 2003, 216-218.
- [44]. B. Yutika, K. Balasubramanian, G. Rohit, Cost-effective, Low Density, Carbon Soot Doped Resorcinol Formaldehyde Composite for Ablative Applications, *RSC Adv.*, 5, 2015, 23622-23634.
- [45]. P. Scherrer, Bestimmung der Grosse und der Inneren Struktur von Kolloidteilchen Mittels Rontgenstrahlen, *Nachrichten von der Gesellschaft der Wissenschaften, Mathematisch-Physikalische Klasse*, 1918, 1918, 98-100.
- [46]. A.C. Ferrari, D.M. Basko, Raman Spectroscopy as a Versatile Tool for Studying the Properties of Graphene, *Nat. Nanotechnol.*, 8, 2013, 235-246.

- [47]. A.C. Ferrari, Raman Spectroscopy of Graphene and Graphite: Disorder, Electron-phonon Coupling, Doping and Nonadiabatic Effects, *Solid State Commun.*, 143, 2007, 47–57.
- [48]. S.J. Kim, Y.J. Park, E.J. Ra, K.K. Kim, K.H. An, Y.H. Lee, Defect-induced Loading of Pt Nanoparticles on Carbon Nanotubes, *Appl. Phys. Lett.*, 90, 2007, 1-3.
- [49]. W.M. Haynes, *CRC Handbook of Chemistry and Physics*, (London UK, CRC Press, 2010)
- [50]. T.F. Otero, J.G. Martínez, K. Asaka, *Front. Mater.*, 3, 2016, 1-17.
- [51]. Ch.T. Hsieh, J.Y. Lin, Fabrication of Bimetallic Pt–M (M= Fe, Co, and Ni) Nanoparticle/carbon Nanotube Electrocatalysts for Direct Methanol Fuel Cells, *J. Power Sources.*, 188, 2009, 347–352.

D. Macias Ferrer "Pt, Co, Fe and Ni Nan particles on Micro/Nano-Structured Carbon for the Methanol Electro-Oxidation in Acid American Journal of Engineering Research (AJER), vol. 7, no. 06, 2018, pp. 344-356.